J MATER RES TECHNOL. 2019;xxx(xx):xxx–xxx

Available online at www.sciencedirect.com

jmr&t Journal of Materials Research and Technology

www.jmrt.com.br

Original Article

Electrochemical analysis of SiC composite additions at 7.5% weight content on the corrosion resistance of monolithic aluminium alloy in sulphate–chloride solution

Roland Tolulope Loto *, *Phillip Babalola*

Department of Mechanical Engineering, Covenant University, Ota, Ogun State, Nigeria

ARTICLE INFO

Article history:
Received 2 January 2019
Accepted 27 March 2019
Available online xxx

Keywords:
Pitting
Corrosion
SiC
Aluminium

ABSTRACT

Effect of specific SiC particle sizes on the corrosion resistance and metastable pitting behaviour of AA1060 aluminium at 7.5% SiC weight content in 0.05 M H_2SO_4, 0.3 M NaCl and 0.05 M H_2SO_4/0.3 M NaCl solution was studied with potentiodynamic polarization, open circuit potential measurement and optical microscopy. SiC slightly increased the susceptibility of aluminium matrix composite (AA1060/SiC) at 9 μm and 29 μm in H_2SO_4 and NaCl solutions. The lowest corrosion rate values were observed at 3 μm and 45 μm SiC particle size. Two metastable pitting portions were visible on the polarization plots at these particles sizes due to passivation and re-initiation of transient corrosion pits. The metastable pitting portion of the polarization plots for AA1060/SiC in H_2SO_4 varied over wider corrosion potential and higher corrosion current compared to the plots from NaCl solution. The relatively smooth transition of the polarization plots in NaCl from anodic polarization to metastable pitting activity of the matrix composite resulted in more concentrated localized corrosion. The effect of SiC particle sizes in the admixed H_2SO_4–NaCl solution significantly contrasts the earlier observations. The OCP plots in H_2SO_4 and NaCl solution shows AA1060/SiC at 45 μm was most electropositive due to the combined action of the protective oxide from aluminium and insulating properties of SiC. The plots at 0 μm for both solutions were comparatively electronegative. Morphological damage of AA1060/SiC at 0 μm was significantly more than the deterioration at 3 μm and 45 μm.

1. Introduction

Metal matrix composites (MMC) are alloys reinforced with metallic and non-metallic particulates such as silicon carbide (SiC), alumina, boron, fly-ash, titanium carbide, etc. The particulates enhance the properties of the substrate metal to cater for the extreme requirements in different engineering applications [1]. Aluminium (Al) is an important manufacturing material in almost all industrial application and processes. It is the most abundant metal and can be processed from its ore at relatively low cost. Research on Al matrix composites (AMC) has shown the huge advantages it has over the monolithic metal due to its homogeneous and isotropic material properties. AMC have been widely applied in

* *Corresponding author.*
E-mail: tolu.loto@gmail.com (R.T. Loto).

https://doi.org/10.1016/j.jmrt.2019.03.001

Please cite this article in press as: Loto RT, Babalola P. Electrochemical analysis of SiC composite additions at 7.5% weight content on the corrosion resistance of monolithic aluminium alloy in sulphate–chloride solution. J Mater Res Technol. 2019. https://doi.org/10.1016/j.jmrt.2019.03.001

Table 1 – Chemical composition (wt.%) of AA1060 aluminium Ingot.

Element	Si	Fe	Cu	Mn	Mg
Composition (%)	0.086	0.281	<0.0002	<0.0005	0.0016
Element	Be	Bi	Ca	Cd	Na
Composition (%)	0.0003	<0.0010	0.0007	0.0002	0.0002
Element	B	P	Pb	Sn	Al
Composition (%)	0.0004	<0.0010	<0.0005	<0.0010	99.6
Element	Cr	Ni	Zn	Ti	Ag
Composition (%)	0.002	0.0023	0.0014	0.0097	<0.0001
Element	Sr	V	Zr	Co	Li
Composition (%)	0.0001	0.0079	0.0021	<0.0010	<0.0001

electronics, automotive, aerospace, bicycles, agricultural machineries etc. for structural applications, electrical conductivity and production of complex engineering parts due to their high strength to weight ratio, stiffness and low density compared to ferrous alloys [2,3]. Research has focused significantly on the physical, mechanical, tribological, manufacturing processes and wears properties of these materials [4–6]. The influence of these composites on the corrosion resistance of AMC is still debatable with no specific consensus. More research needs to be performed to study the localized electrochemical reactions between the composite reinforcements and substrate Al alloy due to the incidence of electrochemical and chemical reactions [7,8]. Addition of composite reinforcements to Al results in discontinuities in the oxide film causing increase in pitting corrosion, rendering the composite liable to severe attack. The major factors that affects the processing outcomes of AMC are interfacial reaction between composite constituents, wettability, the dimension and volume fraction of composite material volume, crevices at the matrix/strengthening interface, fabricating defects, interior stress, microstructural changes and galvanic properties due to link of the matrix and strengthening [9]. Galvanic action between the intermetallic components is majorly responsible for deterioration of the matrix composites. Corrosion significantly weakens the load-bearing capacity of structures causing disastrous failures. The extensive application of AMC enables their exposure of aggressive industrial environments that aggravate corrosion reactions and surface deterioration of the MMC materials. SiC particulate has been known to enhance the mechanical and physical properties of aluminium alloys. Due to its chemical compatibility and formation an adequate bond with the substrate aluminium metal, SiC do not form intermetallic phase within the matrix composite microstructure. However, higher weight percentage composition of SiC causes increased porosity in the microstructure [10,11]. Research into AMC has shown that reinforcement content and particle size strongly influences the corrosion resistance of the material [12-15]. In view of the above this research aims to study the effect of variation of SiC particle size on the corrosion resistance of Al matrix composite at 7.5% SiC weight content.

2. Experimental methods

2.1. *Materials and preparation*

AA1060 aluminium metal (AA1060) was sourced from Aluminium Rolling Mills, Ota, Ogun State, Nigeria. Energy dispersive spectrometer analysis was performed at Materials Characterization Laboratory, Department of Mechanical Engineering, Covenant University, Ota, Ogun State, Nigeria with PhenomWorld characterization device (Model No. MVE0224651193) which gave nominal (wt.%) composition shown in Table 1. Silicon carbide (SiC) at 3 μm, 9 μm, 29 μm and 45 μm particle size with nominal (wt.%) composition shown in Table 2 was purchased from Logitech, UK and added to AA1060 at equal weight percentage of 7.5%. The grit size of SiC particle sizes are shown in Table 3. Stir casting technique was used to produce the aluminium silicon matrix composites (AA1060/SiC). 5 kg of 1060 aluminium metal was liquefied after heating to 750 °C in a graphite crucible within a tilting furnace powered with diesel fuel. The temperature of the molten aluminium was determined with the aid of K-type thermocouple. Molten aluminium was subsequently discharged into mould preheated to 450 °C. The melt was stirred with a mechanical stirrer to give a fine vortex. Silicon carbide particles (SiC) at 7.5 vol. wt% (preheated to 1100 °C) were mix with the vortex at 500 rpm for approximately 5 min. The process was repeated for AA1060/SiC at particle sizes of 3 μm, 9 μm, 29 μm and 45 μm with the same weight percentage (7.5 wt.%). The AA1060/SiC specimens produced through the stir casting method are of cylindrical shape with diameter of 110 mm and height of 30 mm. Their mechanical test results are shown in Table 4. The cast specimens were cut with manual hacksaw after cooling and smoothened with emery papers (80, 320, 600, 800 and 1000 grit). They were subsequently cleansed with deionized water and propanone, and kept in a desiccator for mechanical test, electrochemical test and corrosion potential measurement. Analar grade NaCl purchased from Qualikems, India was prepared in molar concentration of 0.3 M Nacl, while H_2SO_4 acid (analar grade 98%) was prepared in molar concentration of 0.05 M H_2SO_4 with deionized.

Table 2 – Chemical composition (wt.%) of SiC.

Element	C	Al	Fe	Si	SiO_2	Magnetic iron	SiC
Comp. (%)	0.5	0.3	0.2	0.8	0.6	0.04	97.6

Table 3 – Grit size of SiC particle sizes.

Particle size (μm)	Grit size
3	1200
9	600
29	320
45	240

Please cite this article in press as: Loto RT, Babalola P. Electrochemical analysis of SiC composite additions at 7.5% weight content on the corrosion resistance of monolithic aluminium alloy in sulphate–chloride solution. J Mater Res Technol. 2019. https://doi.org/10.1016/j.jmrt.2019.03.001

Table 4 – Mechanical test results for AA1060/SiC (0 μm, 3 μm, 9 μm, 29 μm and 45 μm) on modulus of elasticity, hardness values and electrical conductivity.

Particle size of AA1060/SiC specimen (μm)	Modulus (N/mm^2)	Hardness (HV)	Electrical conductivity (S/m)
0	402.41	19.6	70.254
3	935.03	33.65	63.453
9	1326.21	33.65	65.262
29	760.36	26.05	59.826
45	1517.59	24.75	64.147

2.2. *Potentiodynamic polarization test*

Potentiodynamic polarization was performed on AA1060/SiC specimens with SiC particle sizes of 0 μm, 3 μm, 9 μm, 29 μm and 45 μm. Platinum was used as the counter electrodes, Ag/AgCl as the reference electrodes and resin embedded AA1060/SiC as the working electrodes. The electrodes were placed within a glass container filled with 200 mL of electrolyte solution at 0.05 M H_2SO_4 and 0.3 M NaCl and connected to Digi-Ivy 2311 potentiostat. Polarization curves were produced at scan rate of 0.0015 V/s from −1.35 V and +1.75 V. Corrosion rate, C_{RC} (mm/y) was calculated from the formula below:

$$C_R = \frac{0.00327 \times C_d \times E_q}{D} \quad (1)$$

D is the density in (g/cm^3); E_q is the equivalent weight (g). 0.00327 is the constant for corrosion rate.

2.3. *Open circuit potential (OCP) measurement and optical microscopy characterization*

OCP measurements were performed at a step potential of 0.1 V/s for 3600 s in H_2SO_4 and NaCl solution with two-electrode electrochemical cell consisting of Ag/AgCl reference electrode and resin mounted AA1060/SiC working electrode linked to Digi-Ivy 2311 potentiostat. Optical images of AA1060/SiC surface morphologies at 0 μm, 3 μm and 45 μm was analyzed with Omax trinocular metallurgical microscope.

2.4. *Mechanical test*

Instron universal testing machine (Model 3369) with 30 kN load (ASTM International E8/E8M-09) was used for the tensile test. AA1060 specimens for the test have a cross sectional dimension of 5 mm × 10 mm and a gauge length of 25 mm; five measurements (modulus) were taken per specimen with the mean value used for the result. Microhardness measurements were performed with the aid of LECO 700AT micro harness tester with a load of 492.3 mN and a dwell time of 10 s (ASTM Standard E 384). AA1060/SiC specimen surfaces was polished with emery papers up to 1000 grit sit. Six measurements were taken per specimen with the mean result used as the microhardness value. Electrical conductivity testing was performed with AA1060/SiC specimens with cross sectional dimensions of 10 mm × 10 mm and length of 100 mm using a 4 point probe Keithley instruments machine (Model 2400) with a working voltage is 20 mV. Voltage, current, resistivity and conductivity were obtained the test.

3. Results and discussion

3.1. *Potentiodynamic polarization studies*

Potentiodynamic polarization plots for AA1060/SiC matrix composite (0 μm, 3 μm, 9 μm, 29 μm and 45 μm SiC particle sizes) in 0.05 M H_2SO_4, 0.3 M NaCl and 0.05 M H_2SO_4/0.3 M NaCl solution are shown from Fig. 1(a)–(c). Table 5 shows the data obtained from the polarization test. Observation of the corrosion rate results shows the combined action

Table 5 – Polarization data for AA1060/SiC corrosion in H_2SO_4 and NaCl solution at 0 μm, 3 μm, 9 μm, 29 μm and 45 μm.

SiC content (%)	Corrosion rate (mm/y)	Corrosion current (A)	Corrosion current density (A/cm^2)	Corrosion potential (V)	Polarization resistance, R_p (?)	Cathodic Tafel slope, B_c (V/dec)	Anodic Tafel slope, B_a (V/dec)
0.05 M H_2SO_4							
0	0.112	6.62E−06	1.03E−05	−1.084	3884	−5.105	6.228
3	0.080	4.72E−06	7.37E−06	−1.041	5480	−5.472	5.954
9	0.141	8.32E−06	0.000013	−1.173	3089	−5.429	7.052
29	0.143	8.45E−06	1.32E−05	−1.154	3002	−6.518	3.586
45	0.091	5.36E−06	8.37E−06	−1.021	5463	−5.101	1.487
0.3 M NaCl							
0	0.021	1.23E−06	1.92E−06	−0.963	20,880	−5.501	3.341
3	0.014	8.17E−07	1.28E−06	−1.057	26,540	−6.33	3.884
9	0.023	1.38E−06	2.15E−06	−0.976	18,660	−6.155	5.952
29	0.023	1.38E−06	2.15E−06	−1.053	20,000	−4.689	8.343
45	0.015	8.57E−07	1.34E−06	−1.063	26,240	−7.087	4.997
0.05 M H_2SO_4/0.3 M NaCl							
0	0.875	5.16E−05	8.06E−05	−0.979	498	−3.427	20.1
3	0.438	2.59E−05	4.04E−05	−1.027	993.7	−3.652	17.88
9	0.650	3.83E−05	5.99E−05	−1.021	670.3	−1.572	29.26
29	1.262	7.45E−05	0.000116	−1.016	345	−3.335	18.73
45	1.049	6.19E−05	9.67E−05	−0.758	513.7	−10.19	28.56

Please cite this article in press as: Loto RT, Babalola P. Electrochemical analysis of SiC composite additions at 7.5% weight content on the corrosion resistance of monolithic aluminium alloy in sulphate–chloride solution. J Mater Res Technol. 2019. https://doi.org/10.1016/j.jmrt.2019.03.001

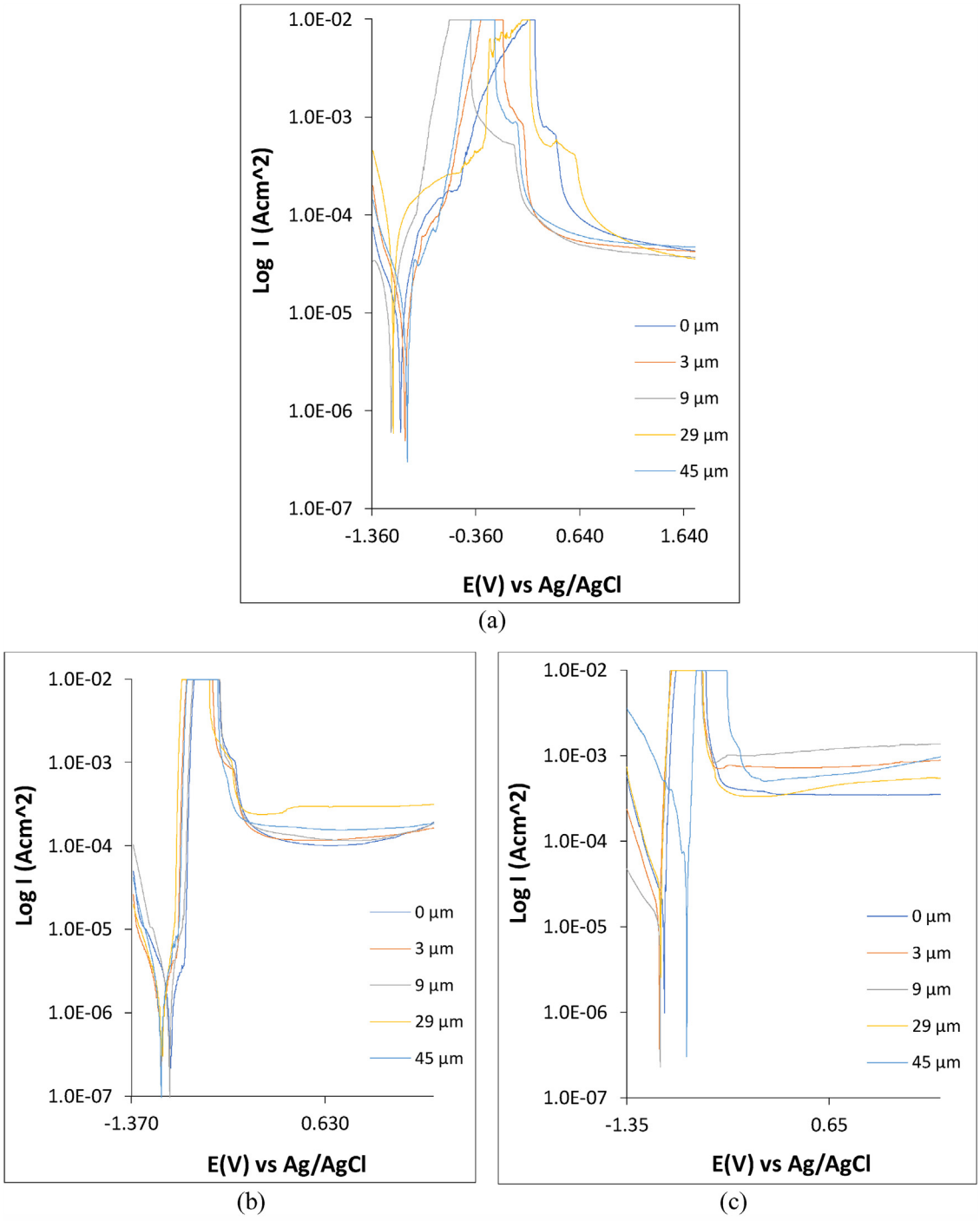

Fig. 1 – Potentiodynamic polarization plots of for AA1060/SiC corrosion at 0 µm, 3 µm, 9 µm, 29 µm and 45 µm (a) H_2SO_4, (b) NaCl and (c) H_2SO_4/NaCl solution.

of sulphate/chloride anions are generally more destructive to the surface oxide film followed by the sulphate anions, leading to anodic dissolution of the matrix composite. Significant differences in polarization resistance value confirm this assertion. In the electrolytes, the corrosion rate of AA1060/SiC (0–3 µm) decreased from 0.875 mm/y to 0.438 mm/y in H_2SO_4/NaCl, 0.112 mm/y to 0.080 mm/y in H_2SO_4, and 0.021 mm/y to 0.014 mm/y in NaCl. This corresponds to corrosion current density of 4.04×10^{-5} A cm^{-2}, 7.37×10^{-6} A cm^{-2} and 1.28×10^{-6} A cm^{-2} in both solutions at 3 µm, 9 µm and 29 µm SiC particle sizes tend to increase the susceptibility of AA1060/SiC to corrosion. The discontinuities on AA1060/SiC surface at these larger SiC particle sizes result in galvanic reactions between the intermetallic phases, precipitates and impurities within the metallurgy of the substrate aluminium metal causing selective deterioration of AA1060/SiC in NaCl solution as shown in the negative shift in corrosion potential despite similar corrosion

Please cite this article in press as: Loto RT, Babalola P. Electrochemical analysis of SiC composite additions at 7.5% weight content on the corrosion resistance of monolithic aluminium alloy in sulphate–chloride solution. J Mater Res Technol. 2019. https://doi.org/10.1016/j.jmrt.2019.03.001

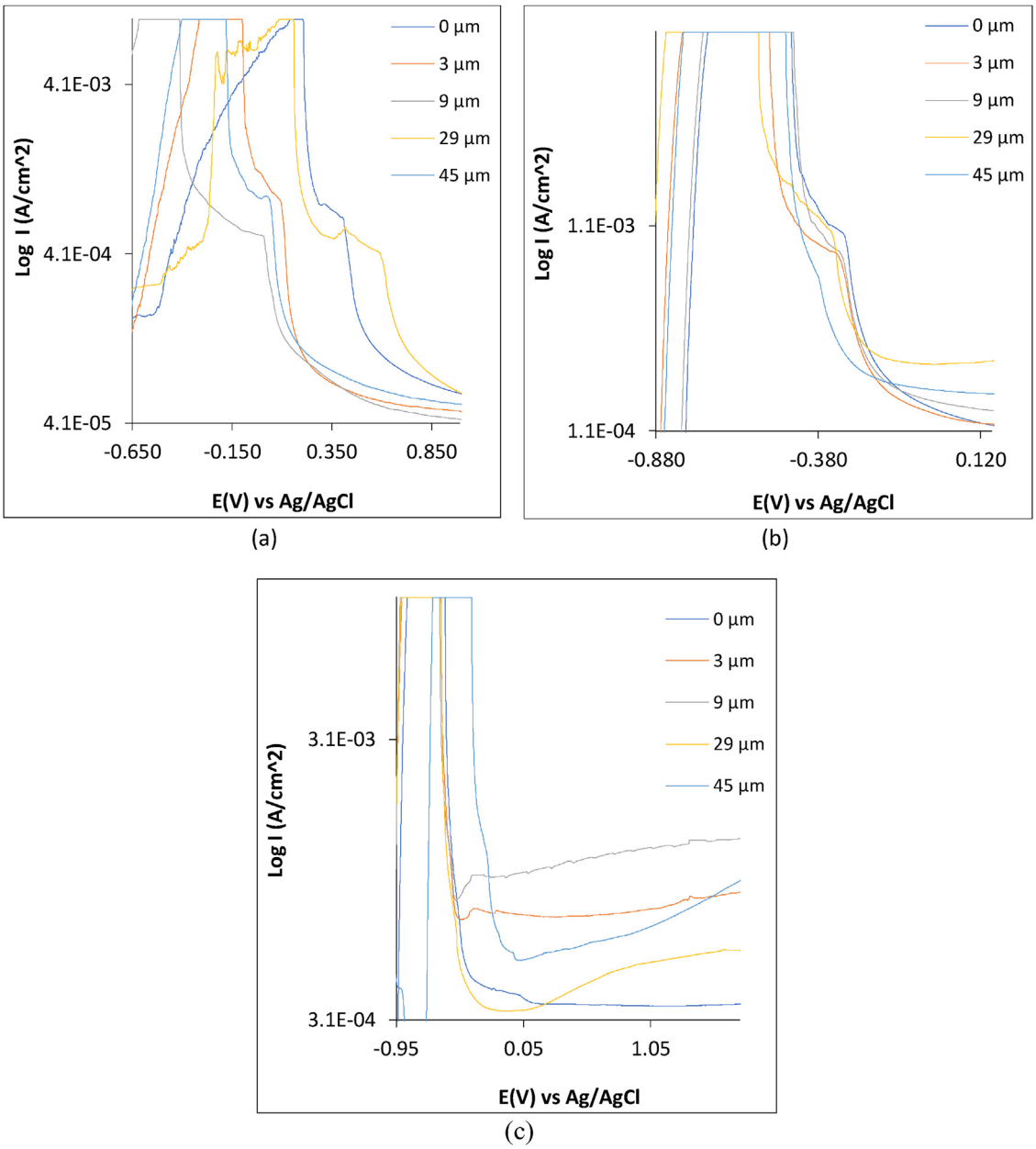

Fig. 2 – Close-up view of the potentiodynamic polarization plot 0f 1060/SiC (0 µm, 3 µm, 9 µm, 29 µm and 45 µm particle sizes) showing the metastable pitting and repassivation regions of the plots (a) H_2SO_4 solution, (b) NaCl solution and (c) H_2SO_4/NaCl solution.

rates. In H_2SO_4, the destructive effects of sulphate anions result in anodic dissolution from observation of the positive shift in corrosion potential and increase in corrosion rate. In the presence of sulphate/chloride admixture, the rate of corrosion is higher coupled with a positive shift in corrosion potential as earlier observed in H_2SO_4 solution. However, at 45 µm the corrosion rate of AA1060/SiC decreases to 1.049 mm/y, 0.091 mm/y and 0.015 mm/y in H_2SO_4/NaCl, H_2SO_4 and NaCl solution. The positive shift in corrosion potential of AA1060/SiC in H_2SO_4 at 3 µm and 45 µm particle size is due to anodic inhibition effect of SiC at the respective particle sizes resulting in enhanced corrosion resistance of AA1060/SiC. In NaCl, the corrosion potential shifts to negative values at 3 µm and 45 µm particle sizes signify cathodic inhibition of the oxygen reduction and hydrogen evolution reactions occurring on AA1060/SiC surface. In H_2SO_4/NaCl solution, the shift in corrosion potential is due to competitive action of chlorides and sulphates on the matrix surface resulting in cathodic inhibition at 3 µm and anodic inhibition at 45 µm. The similarities in the cathodic and anodic Tafel slope of AA1060/SiC in NaCl, and the cathodic Tafel slope in H_2SO_4 shows the corrosion mechanism is under activation control. Significant changes in the anodic Tafel slope for AA1060/SiC in H_2SO_4 shows anodic dissolution reactions were responsible for the higher corrosion rates of AA1060/SiC resulting in delayed passivation of the matrix composite during

Please cite this article in press as: Loto RT, Babalola P. Electrochemical analysis of SiC composite additions at 7.5% weight content on the corrosion resistance of monolithic aluminium alloy in sulphate–chloride solution. J Mater Res Technol. 2019. https://doi.org/10.1016/j.jmrt.2019.03.001

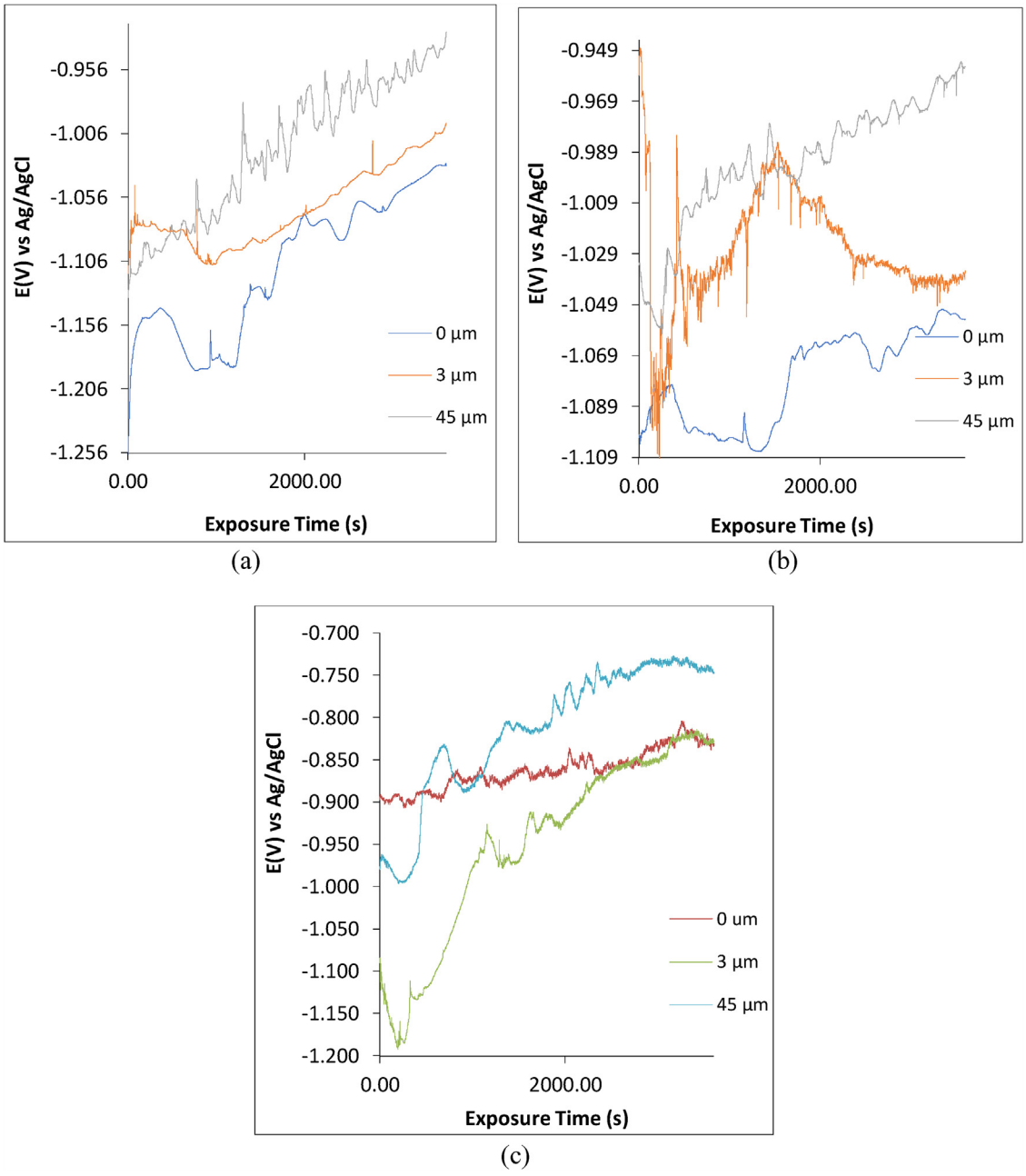

Fig. 3 – Variation of OCP value versus exposure time for AA1060/SiC at 0 µm, 3 µm and 45 µm (a) 0.05 M H_2SO_4, (b) 0.3 M NaCl and (c) 0.05 M H_2SO_4/0.3 M NaCl solution.

potential scanning. The effect of chloride/sulphate admixture is evident on the anodic/cathodic portion of the polarization plot of 1060/SiC (Fig. 1(c)). The increase in anodic slope of the polarization plot shows anodic dissolution reactions dominate the redox electrochemical process. This is confirmed from the positive shifts in corrosion potential after 0 µm SiC particle size and higher anodic Tafel slope values. Between 0 µm and 29 µm SiC particle, the cathodic reaction mechanism is under activation control as shown in similar cathodic polarization plot. However, at 45 µm a significant shift in corrosion potential occurred ($-1.016\,V_{Ag/AgCl}$ to $-0.758\,V_{Ag/AgCl}$) in addition to a large increase in cathodic Tafel slope value to increase in surface impedance as a results of the matrix surface whereby selective deterioration of the matrix composite dominate.

3.2. *Metastable pitting*

Initiation and growth of corrosion pits after anodic polarization, and subsequent repassivation of the weakened oxide film on 1060/SiC matrix composite in sulphate and chloride solutions involve metastable pitting activity which is an important phenomenon in the overall corrosion resistance of 1060/SiC matrix composites. The potentiostatic behaviour of metastable pits is subject to electrolytic transport of discharged metallic cations from within the corrosion pits

Please cite this article in press as: Loto RT, Babalola P. Electrochemical analysis of SiC composite additions at 7.5% weight content on the corrosion resistance of monolithic aluminium alloy in sulphate–chloride solution. J Mater Res Technol. 2019. https://doi.org/10.1016/j.jmrt.2019.03.001

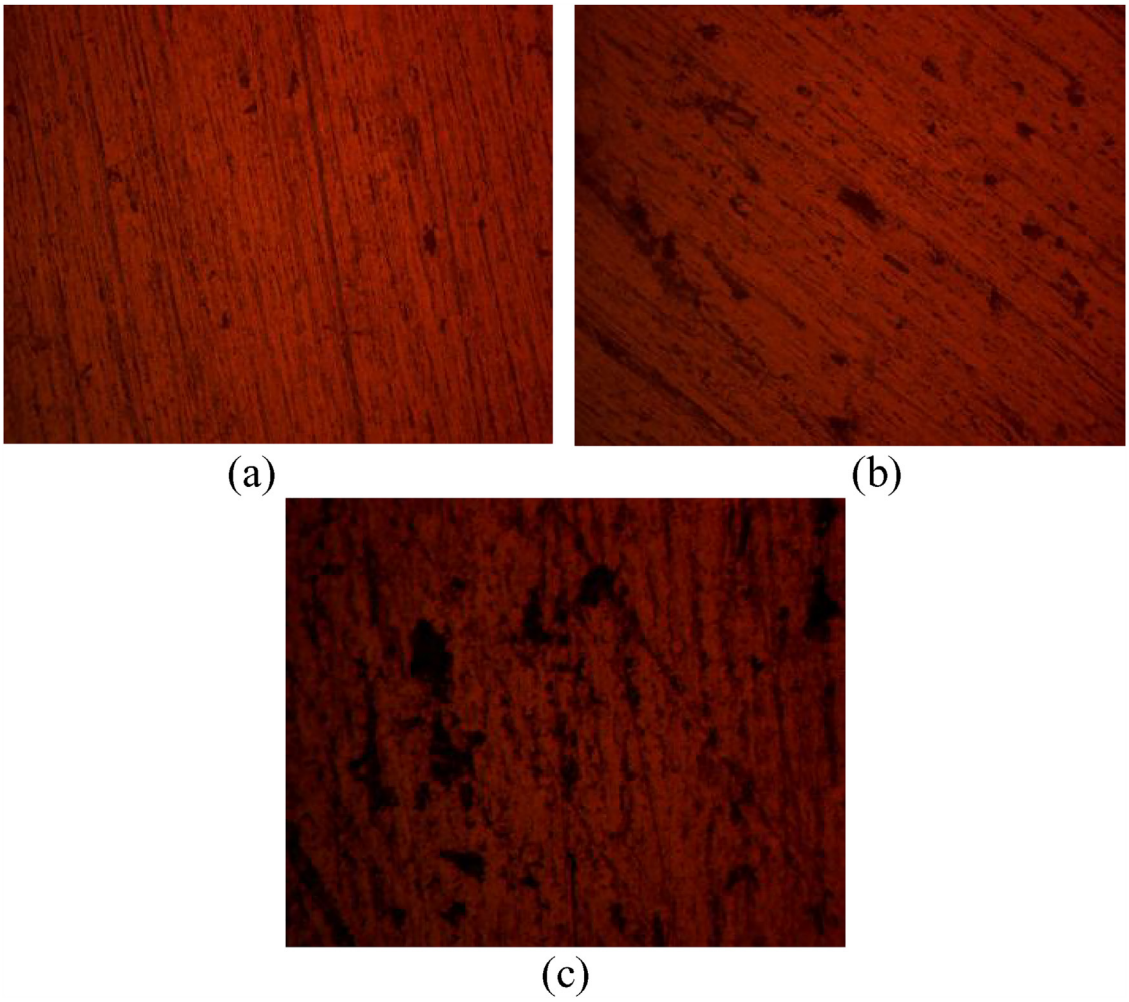

Fig. 4 – Optical image of AA1060/SiC before corrosion (mag. 40×) (a) 0 μm, (b) 3 μm and (c) 45 μm.

and the redox electrochemical reactions occurring on the heterogeneous composite surface. Increased metastable pitting activity delays the formation of the protective oxide. Fig. 2(a)–(c) shows an enlarged magnification of the metastable pitting behaviour and onset of stable passivation on the polarization plot of 1060/SiC at 0 μm, 3 μm, 9 μm, 29 μm and 45 μm particle sizes in H_2SO_4, NaCl and H_2SO_4/NaCl solutions during potential scanning. Two metastable pitting portions on the polarization plots are visible on both Fig. 2(a) and (b) signifying the passivation and re-initiation of transient corrosion pits before stable passivation. This delays the reformation of the protective oxide on 1060/SiC matrix composite at all particle sizes studied. The metastable pitting portion of the polarization for 1060/SiC in 0.05 M H_2SO_4 (Fig. 2(a)) varies over wider corrosion potential and current compared to the plot from 0.3 M NaCl solution (Fig. 2(b)). This is due to greater surface deterioration of the matrix composite as shown in the anodic portion of the plot, in addition to localized reactions responsible for the limited propagation of corrosion pits. The resultant effect of this phenomenon is the delayed repassivation of the matrix composite in H_2SO_4 solution compared to NaCl solution. It is clearly visible that sulphate anions cause pitting corrosion. However, the small size of chloride anions allows for easier diffusion through the protective film resulting in more concentrated localized corrosion. This is evident from the relatively smooth transition of the polarization plots from anodic polarization to metastable pitting activity and the repassivation of the matrix composite at lower corrosion current. The polarization plot in Fig. 2(c) shows only one metastable pitting portion due to the combine action of chlorides and sulphates, as a result there is no transient repassivation during metastable pitting activity. Comparing the metastable pitting plot in Fig. 2(a) and (b) show that AA1060/SiC repassivate at higher corrosion current density in the presence of chlorides. This phenomenon is due to the higher reactive nature of chlorides and the autocatalytic nature of the pitting corrosion process. While chlorides may not be as deleterious on the surface of matrix composites from observation of the corrosion rate results, it diffuses easily through the protective oxide, significantly deteriorating limited portions of the composite. Sulphates do cause pitting, but on a slightly lower scale than chlorides. The effect of chlorides tends to be general surface deterioration. Observation of the metastable pitting plot in Fig. 2(c) shows the combine corrosive species increases the tendency for pitting corrosion. Repassivation occurred at higher corrosion current density than in Fig. 2(b).

Please cite this article in press as: Loto RT, Babalola P. Electrochemical analysis of SiC composite additions at 7.5% weight content on the corrosion resistance of monolithic aluminium alloy in sulphate–chloride solution. J Mater Res Technol. 2019. https://doi.org/10.1016/j.jmrt.2019.03.001

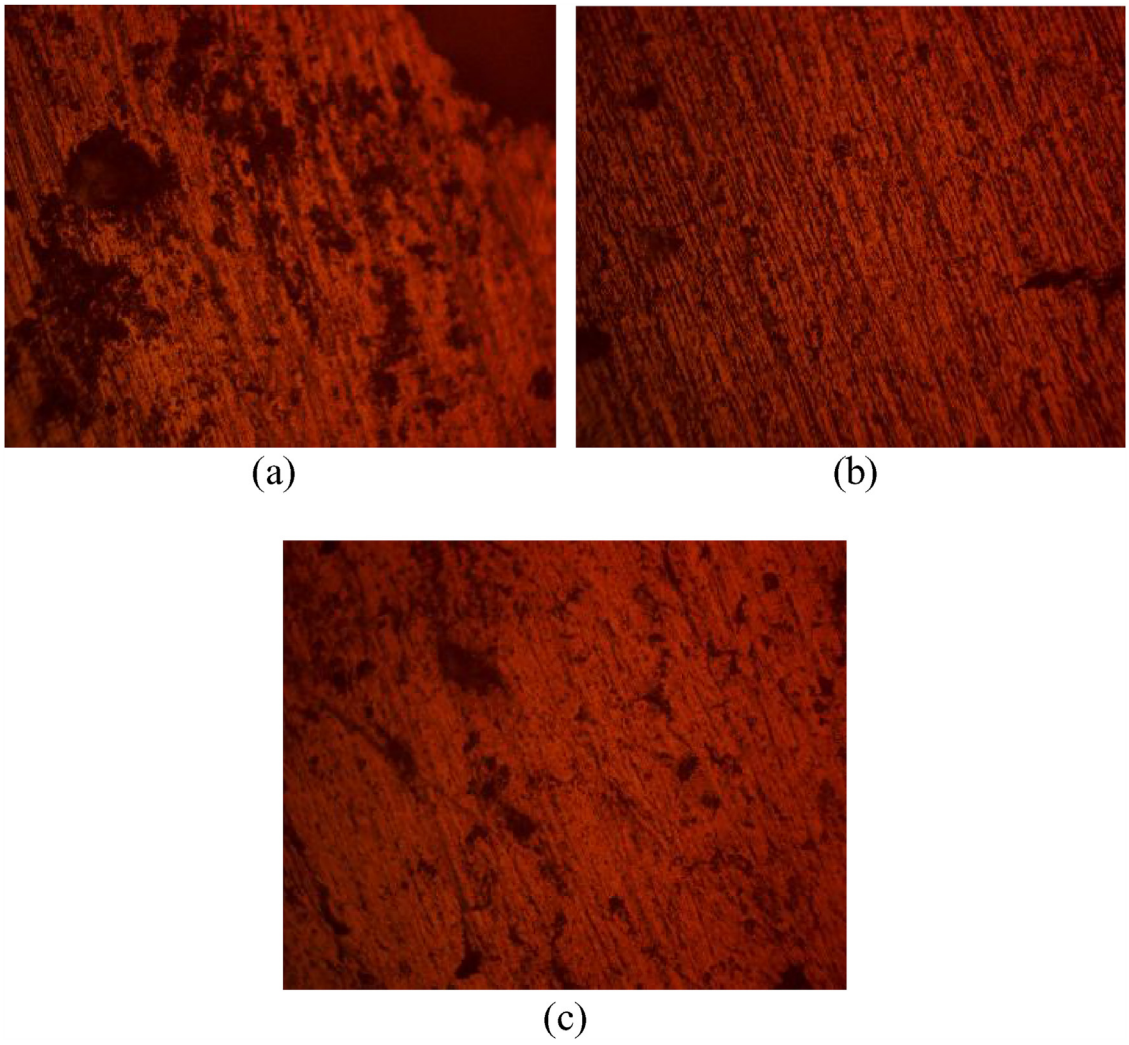

Fig. 5 – Optical image of AA1060/SiC after corrosion in 0.05 M H_2SO_4 (mag. 40×) (a) 0 μm, (b) 3 μm and (c) 45 μm.

3.3. *Open circuit potential measurement (OCP)*

Variation of OCP values versus exposure time for AA1060/SiC in H_2SO_4, NaCl and H_2SO_4/NaCl solution at 0 μm, 3 μm and 45 μm SiC particle sizes are shown in Fig. 3(a)–(c). The OCP plots in the figures shows AA1060/SiC at 45 μm is the most electropositive though in H_2SO_4/NaCl solution, the corrosion potential values of AA1060/SiC are the most electropositive due to formation of more resilient protective oxide. However, the OCP plots from the electrolyte attained relative stability at 2803 s till the end of the exposure period. The OCP plots of AA1060/SiC at 0 μm SiC particle size are the most electronegative. This observation agrees with the corrosion rate results from polarization test. The position of plots at 45 μm in Fig. 3(a)–(c) is due to the enhanced corrosion resistance of AA1060/SiC in the presence of larger SiC particle sizes. However, the active–passive behaviour is due to the breakdown and repassivation of the discontinuous oxide film on the matrix composite because of galvanic action on the heterogeneous surface. Nevertheless, the thermodynamic instability has no significant effect on the corrosion resistance of AA1060/SiC as the plots continue to proceed towards electropositive values till the end of the exposure period. The OCP plot of AA1060/SiC at 3 μm in Fig. 3(a) and (c) proves to be more thermodynamically stable in the presence of sulphate and chloride/sulphate anions compared to chlorides anions (Fig. 3(b)) where potential transients are significantly prevalent. Though a significant decrease in corrosion potential was observed between 405.6 s and 800.01 s in Fig. 3(b) (from −1.145 $V_{Ag/AgCl}$ to −1.191 $V_{Ag/AgCl}$) due to anodic dissolution reactions, the electropositive shift in corrosion potential shows the protective film on the matrix composite is relatively resilient in the absence of applied potential. The aggressive nature of chlorides and their ability to initiate pitting is the cause of the potential transients [16–19]. Between 1493.11 s and 3021.52 s, the OCP value of 3 μm (Fig. 3(b)) decreased from −0.978 V_{AgCl} −1.044 V_{AgCl} before attaining relative stability till the end of the exposure period. The protective oxide film throughout its exposure period is unstable compared to Fig. 3(c) where the OCP plot continued to progress to positive values. The OCP plots of AA1060/SiC at 0 μm SiC particle size demonstrated active–passive behaviour (Fig. 3(a) and (b)) in addition to being thermodynamically unstable. The electrochemical action of chlorides (Fig. 3(b)) hindered the growth of the oxide film; hence limits its

Please cite this article in press as: Loto RT, Babalola P. Electrochemical analysis of SiC composite additions at 7.5% weight content on the corrosion resistance of monolithic aluminium alloy in sulphate–chloride solution. J Mater Res Technol. 2019. https://doi.org/10.1016/j.jmrt.2019.03.001

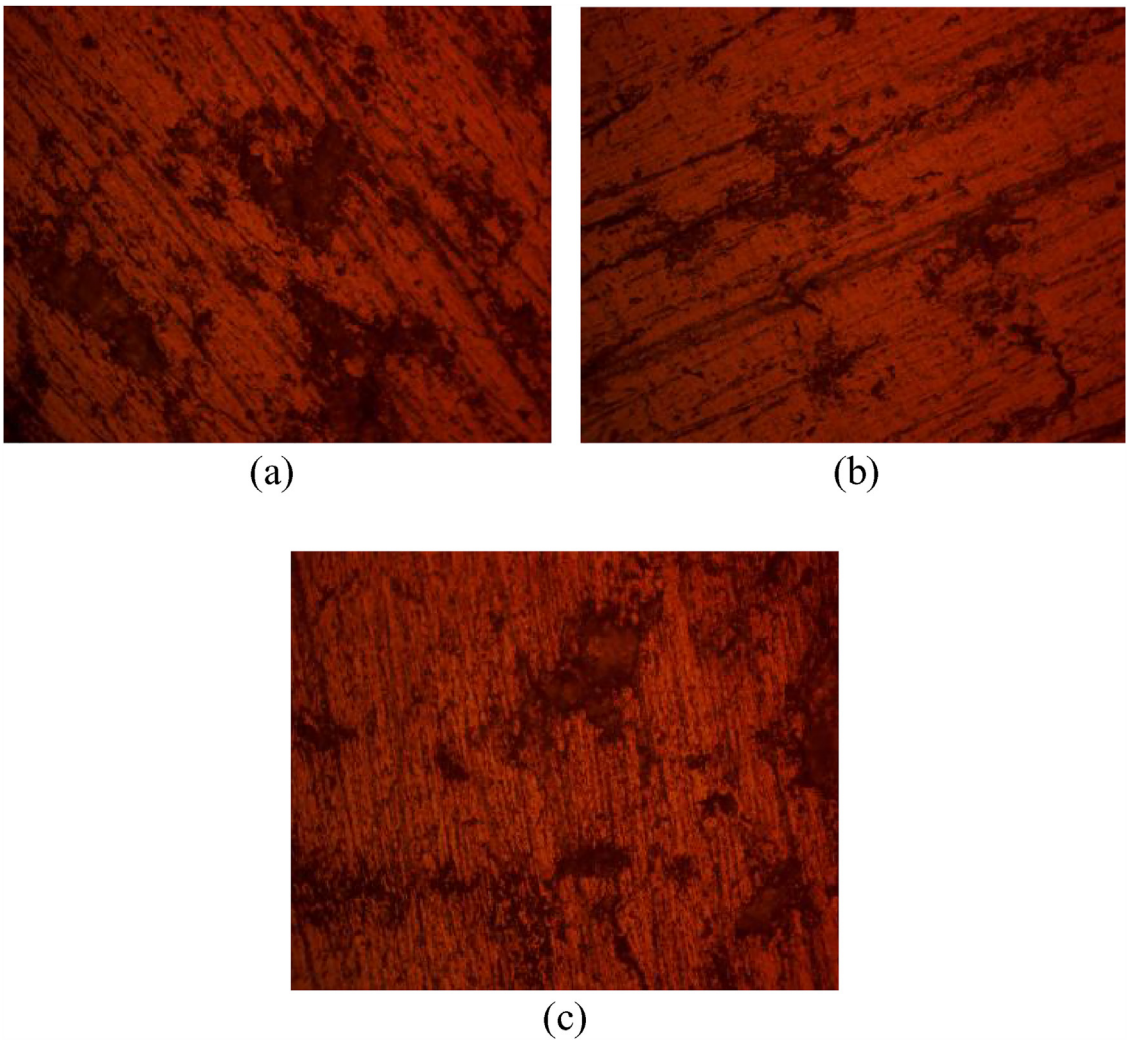

Fig. 6 – Optical image of AA1060/SiC after corrosion in 0.3 M NaCl (mag. 40×) (a) 0 μm, (b) 3 μm and (c) 45 μm.

corrosion resistance in NaCl solution. However, the OCP plot in Fig. 3(c) at 0 μm SiC particle size showed relatively stable thermodynamic behaviour from onset till the end of the exposure period. No positive shift in corrosion potential values was observed in Fig. 3(b) till the end of the exposure period, whereas the plot in Fig. 3(a) shows positive shift in OCP values till the end of the exposure period due to differences in the electrochemical action of sulphate anions. AA1060/SiC proves to be more corrosion resistant in the presence of sulphates only.

3.4. *Optical microscopy analysis*

Optical images of AA1060/SiC (mag. 40×) at 0 μm, 3 μm and 45 μm SiC particle sizes before and after corrosion in 0.05 M H_2SO_4, 0.3 M NaCl and 0.05 M H_2SO_4/0.3 M NaCl solution are shown from Figs. 4(a)–7(c). Fig. 4(a)–(c) shows the optical images of the specimens before corrosion test. The morphologies of the matrix composite specimens are quite different due to the presence of SiC particles at specific sizes. Fig. 5(a)–(c) shows the optical images of AA1060/SiC after corrosion in 0.05 M H_2SO_4 solution. Corrosion pits of various sizes are visible on the morphology of AA1060/SiC at 0 μm (Fig. 5(a)) compared to Fig. 5(b) and (c) due to the presence of SiC particles which limited the diffusion and anodic dissolution of reducible species (due to the electrochemical action of sulphate anions) on the matrix composite surface. While the morphological surface deterioration in Fig. 5(a) reveals the extent of redox electrochemical processes involving sulphate anions, it must be noted that the sulphate anions modifies the chemical properties of the matrix composite surface, weakening it and causing the release of metal ions into the electrolyte [20,21]. The damages on morphology of AA1060/SiC (Fig. 6(a)–(c)) appear superficial judging from the corrosion rate results and comparing with the morphology from H_2SO_4 solution. However, this is not the case due to the localized corrosion reaction mechanism usually exhibited by chlorides anions on metallic surfaces. Chloride anions adsorbs on the surface of the passive oxide due to the net positive charge on the matrix composite surface in the electrolyte. This adsorption leads to concentration of chloride anions at specific sites on the matrix composite resulting the formation of local anode sites due to hydrolysis reaction [22,23]. The extent of damage in Fig. 6(a) is relatively higher than Fig. 6(b) and (c) due

Please cite this article in press as: Loto RT, Babalola P. Electrochemical analysis of SiC composite additions at 7.5% weight content on the corrosion resistance of monolithic aluminium alloy in sulphate–chloride solution. J Mater Res Technol. 2019. https://doi.org/10.1016/j.jmrt.2019.03.001

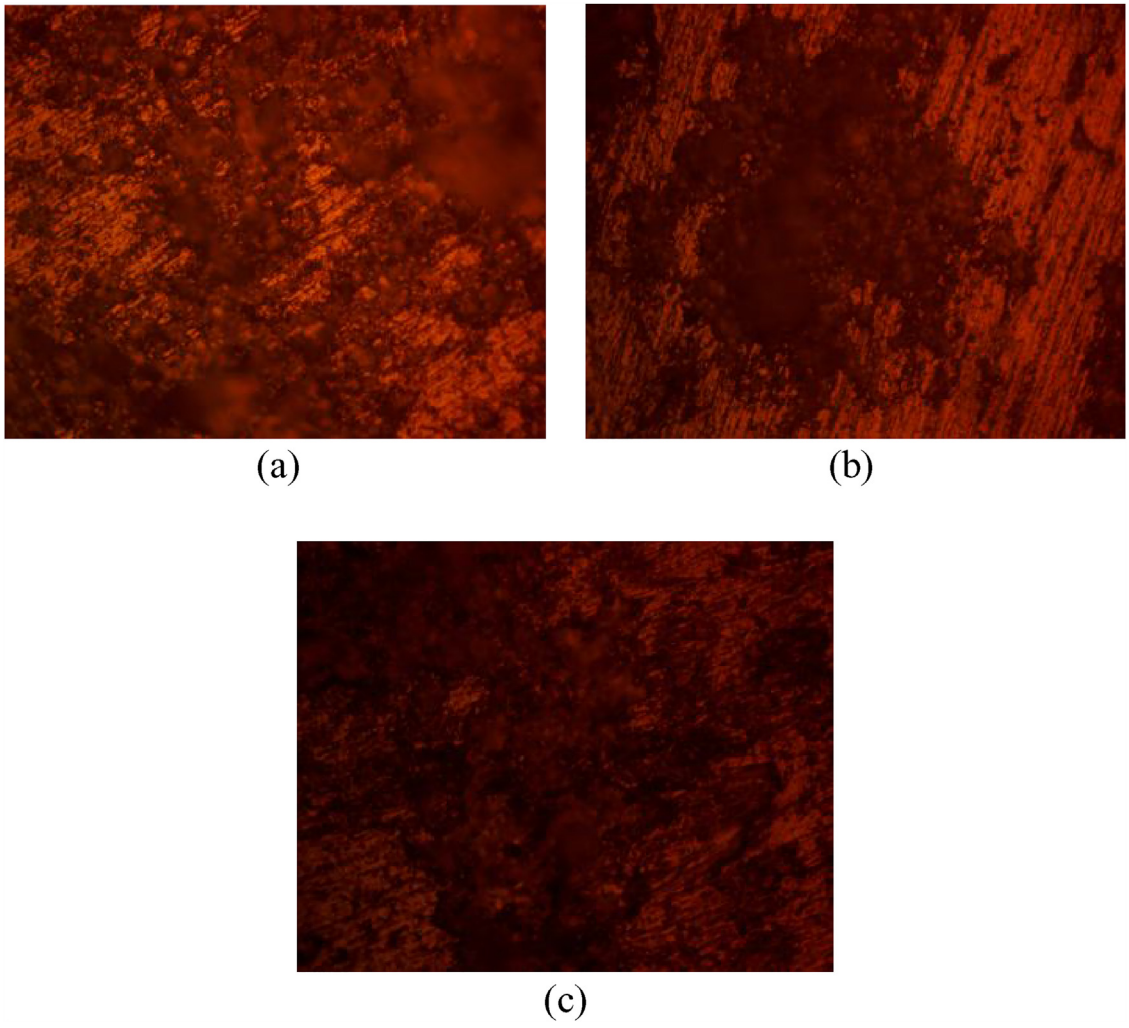

Fig. 7 – Optical image of AA1060/SiC after corrosion in 0.05 M H_2SO_4/0.3 NaCl (mag. 40×) (a) 0 μm, (b) 3 μm and (c) 45 μm.

to the absence of SiC. Observation of Fig. 7(a)–(c) shows chloride/sulphate admixture has more deleterious effect on the morphology of AA1060/SiC compared to the previous electrolytes studied. The morphological damage agrees with the higher corrosion rate result obtained for the matrix composite in 0.05 M H_2SO_4/0.3 NaCl solution. Analysis of the surfaces shows the extent of damage to be less for the morphology at 3 μm, while the damage on the morphology at 45 μm was the most extensive. Irrespective of the SiC particle size the admixture of the corrosive species is detrimental to the protective oxide film on AA1060/SiC.

4. Conclusions

Electrochemical study of the effect of SiC particle size on the corrosion resistance of aluminium silicon carbide matrix composite at 7.5% SiC weight content in sulphate and chloride solutions showed the matrix composite is more corrosion resistant at the lowest and highest SiC particle sizes (3 μm and 45 μm). Though the extent of deterioration is generally much higher in the sulphate solution, anodic corrosion inhibition was observed at 3 μm particle size while cathodic corrosion inhibition was observed at 45 μm particle size. Formation of transient corrosion pits on the matrix composite in H_2SO_4 solution occurred at higher corrosion current over wide corrosion potential due to the aggressive action of sulphates. Optical images showed the morphological deterioration of the matrix composite in NaCl is more concentrated compared to general surface deterioration on the morphology from H_2SO_4 solution. This is related to the smooth transition of the polarization plots from anodic polarization to metastable pitting activity in chloride solution. Open circuit potential plots show the matrix composite at 45 μm is the more electropositive due to its higher corrosion resistance and formation of resilient oxide film.

Conflicts of interest

The authors declare no conflicts of interest.

Please cite this article in press as: Loto RT, Babalola P. Electrochemical analysis of SiC composite additions at 7.5% weight content on the corrosion resistance of monolithic aluminium alloy in sulphate–chloride solution. J Mater Res Technol. 2019. https://doi.org/10.1016/j.jmrt.2019.03.001

Acknowledgements

The authors acknowledge Covenant University, Ota, Ogun State, Nigeria for the sponsorship and provision of research facilities for this project.

REFERENCES

[1] Vijaya RB, Elanchezhian C, Annamalai RM, Aravind ST, Sri Ananda TA, Vignesh V, et al. Aluminium metal matrix composites – a review. Rev Adv Mater Sci 2014;38:55–60.
[2] Sahin Y, Acilar M. Production and properties of SiCp-reinforced aluminium alloy composites. Composites A Appl Sci Manuf 2003;34:709–18.
[3] Hassan AM, Mayyas AT, Alrashdan A, Mohammed T, Hayajneh MT. Wear behavior of Al–Cu and Al–Cu/SiC components produced by powder metallurgy. J Mater Sci 2008;43:5368–75.
[4] Karvanis K, Fasnakis D, Maropoulos A, Papanikolaou S. Production and mechanical properties of Al–SiC metal matrix composites. IOP Conf Ser Mater Sci Eng 2016;161(1), http://dx.doi.org/10.1088/1757-899X/161/1/012070.
[5] Sijo MT, Jayadevan KR. Analysis of stir cast aluminium silicon carbide metal matrix composite: a comprehensive review. Proc Technol 2016;24:379–85.
[6] Rahman H, Mamun Al Rashed HM. Characterization of silicon carbide reinforced aluminum matrix composites. Proc Technol 2014;90:103–9.
[7] Liu ZS, Huang B, Gu M. Corrosion behavior of Al/AlNp composite in alkaline solution. Mater Lett 2006;60:2024–8.
[8] Durai TG, Das K, Das S. Effect of mechanical milling on the corrosion behavior of Al–Zn/Al_2O_3 composite in NaCl solution. J Mater Sci 2007;42:8209–14.
[9] Mahmoud TS, El-Kady EY, Al-Shihiri ASM. Corrosion behaviour of Al/SiC and Al/Al_2O_3 nanocomposites. Mater Res 2012;15:903–10.
[10] Umanath K, Palanikumar K, Selvamanid ST. Analysis of dry sliding wear behavior of Al6061/SiC/Al_2O_3 hybrid metal matrix composites. Compos B Eng 2013;53:159–68.
[11] Smith AV. Titanium diboride particle reinforced aluminium with high wear resistance. J Mater Sci 1996;31(22):5961–73.
[12] Loto RT, Babalola P. Effect of alumina nano-particle size and weight content on the corrosion resistance of AA1070 aluminum in chloride/sulphate solution. Results Phys 2018;10:731–7.
[13] Loto RT. Investigation of the localized corrosion resistance of 4044 aluminum alloy in acid chloride and neutral chloride solutions. J Fail Anal Prev 2018;18:905–11.
[14] Loto RT, Babalola P. Analysis of SiC grain size variation and NaCl concentration on the corrosion susceptibility of AA1070 aluminium matrix composites. Cogent Eng 2018;5, http://dx.doi.org/10.1080/23311916.2018.1473002.
[15] Loto RT, Babalola P. Corrosion polarization behavior and microstructural analysis of AA1070 aluminium silicon carbide matrix composites in acid chloride concentrations. Cogent Eng 2017;4, http://dx.doi.org/10.1080/23311916.2017.1422229.
[16] Yang Q, Luo JL. Effects of hydrogen and tensile stress on the breakdown of passive films on type 304 stainless steel. Electrochim Acta 2001;46:851–9.
[17] Phanis SK, Satpati AK, Muthe KP, Vyas JC, Sundaresan RI. Comparison of rolled and heat treated SS304 in chloride solution using electrochemical and XPS techniques. Corros Sci 2003;45:2467–83.
[18] Ameer MA, Fekry AM, El-Taib F, Heakel FE. Electrochemical behaviour of passive films on molybdenum-containing austenitic stainless steels in aqueous solutions. Electrochim Acta 2004;50:43–9.
[19] El-egamy SS, Badway WA. Passivity and passivity breakdown of 304 stainless steel in alkaline sodium sulphate solutions. J Appl Electrochem 2004;34:1153–8.
[20] Al Teyyib AJ, Somuah SK, Booh JK, Leblauc P, Al Mana AJ. Laboratory study on the effect of sulfate ions on rebar corrosion. Cem Concr Res 1988;18:249–56.
[21] Mursalo N, Tullmln M, Robinson FP. The corrosion behavior of mild steel, 3CR12, and AISI type 316L in synthetic mine waters. J South. Afr Inst Min Metall 1988;88:249–56.
[22] McCafferty E. Sequence of steps in the pitting of aluminum by chloride ions. Corros Sci 2003;45:1421–38.
[23] Kamimura T, Kashima K, Sugae K, Miyuki H, Kudo T. The role of chloride ion on the atmospheric corrosion of steel and corrosion resistance of Sn-bearing steel. Corros Sci 2012;62:34–41.

Please cite this article in press as: Loto RT, Babalola P. Electrochemical analysis of SiC composite additions at 7.5% weight content on the corrosion resistance of monolithic aluminium alloy in sulphate–chloride solution. J Mater Res Technol. 2019. https://doi.org/10.1016/j.jmrt.2019.03.001